Autophagy and senescence in primary human bronchial epithelial cells in the context of COPD

Annie Vegraeus

Master's thesis project in Molecular Biology (30cr)

MOBM02

The department of Biology, Lund University

2022-2023

The project was performed at AstraZeneca, Gothenburg.

Supervisors at AstraZeneca:

Svitlana Salemio - Senior Scientist, Target Science Lead

Barry Collins – Associate Principal Scientist, Bioscience

Supervisor at Lund University:

Wolfgang Knecht, Associate Professor, Lund University

Abstract

Chronic obstructive pulmonary disease (COPD) is the third largest cause of death worldwide, with its most prominent risk factor being inhalation of smoke and pollutants. In this project, we studied two processes that are involved in COPD: autophagy and cellular senescence. Using primary human bronchial epithelial cells (HBECs) from healthy and COPD donors, we aimed to show that cigarette smoke extract (CSE) gives rise to an impaired autophagy flux as well as increased senescence. With multiple CSE incubation times and CSE concentrations, our data shows an impaired autophagy flux at the early time points 5h and 24h. However, the senescence data is inconclusive. Further optimization of the study design could enable the development of an appropriate *in vitro* assay. In the end, could continued research of this kind contribute to increased knowledge and understanding of the disease, as well as enable development of medical targets in the mission of disease treatment.

List of abbreviations

AMPK - AMP-activated protein kinase

BCA - bicinchoninic acid

BEGM – bronchial epithelial cell growth basal medium

COPD – chronic obstructive pulmonary disease

CS – cigarette smoke

CSE – cigarette smoke extract

DMEM - Dulbecco's modified eagle medium

DPBS - Dulbecco's phosphate-buffered saline

LC3 - microtubule-associated protein 1A/1B-light chain 3

ECM – extracellular matrix

ER - endoplasmic reticulum

GAPDH - glyceraldehyde 3-phosphate dehydrogenase

HBECs – human bronchial epithelial cells

HCA - high content screening systems

HLFs – human lung fibroblasts

IL-6 – interleukin-6

IL-8 – interleukin-8

MCP-1, -2, -3, -4 – monocyte chemoattractant proteins

MIPs– macrophage inflammatory proteins

mTOR – the mammalian target of rapamycin

mTORC1 - the mammalian target of rapamycin complex 1

mTORC2 - the mammalian target of rapamycin complex 2

PBS - phosphate buffered saline

PFA – paraformaldehyde

PE – phosphatidylethanolamine

PI3P - phospholipid phosphatidylinositol 3-phosphate

PVDF - polyvinylidene fluoride

ROS – reactive oxygen species

SAD – small airway disease

SASP - senescent-associated secretory phenotype

SA-β-Gal - the senescence-associated β-galactosidase

Introduction

Chronic obstructive pulmonary disease

Chronic obstructive pulmonary disease (COPD) is a progressive and incurable respiratory disease, estimated to be the third leading cause of death worldwide (Racanelli, 2017). It involves airway obstruction and increased inflammatory responses in the respiratory tract, with multiple risk factors including increasing age and socioeconomic status as well as multiple comorbidities, e.g. asthma, cardiovascular disease, malnutrition and bronchiectasis (i.e the widening and damaging of the bronchi) (Matsunaga et al., 2020). However, the biggest risk factor for COPD is exposure to cigarette smoke (CS) and other pollutants (Matsunaga et al., 2020; Racanelli, 2017). The compounds in CS have shown to induce oxidative cellular stress, increase inflammation and disrupt cellular homeostasis in the respiratory tract (Rodrigues et al., 2021; Vij et al., 2016).

COPD can be characterized by three disease states: chronic bronchitis, emphysema, and small airway disease (SAD). Chronic bronchitis refers to overproduction of mucus in the proximal airways. Emphysema involves peripheral lung destruction, including destruction of the alveoli and their attachments. SAD is a state which precedes emphysema, occurring in the early stages of COPD. It involves narrowing and destruction of the small airways. (Racanelli, 2017; Rodrigues et al., 2021; Singh, 2017).

Two cellular processes associated with aging and implicated in COPD pathology, are autophagy and senescence (Fujii et al., 2012; Pehote & Vij, 2020; Racanelli, 2017). Autophagy is a constitutive intracellular process involving the degradation of damaged proteins, organelles, and infectious agents such as bacteria and viruses. It is highly important for the homeostasis of the cell (Kuwano, 2016). Cellular senescence occurs when an aging cell goes into a non-dividing state due to cellular damage of different kinds. The cause could be replication, resulting in too large a loss of telomeric ends, or cellular stress with e.g. reactive oxygen species (ROS) production and DNA damage (Kuilman et al., 2010; Wang et al., 2009). Apart from a halt in the cell cycle, the secretory profile of the cell alters as it becomes senescent. This is called the senescent-associated secretory phenotype (SASP). The SASP involves the expression and secretion of different cytokines, chemokines and growth factors, among others (Hamsanathan et al., 2019; Muñoz-Espín & Serrano, 2014).

Both processes have been shown to be implicated in COPD, and they have furthermore been shown to influence each other (Fujii et al., 2012; Vij et al., 2016). The two processes will now be described in more detail.

Autophagy

Autophagy acts through lysosomal degradation and functions to maintain and regulate the synthesis, degradation and removal of cellular components (Kuwano, 2016; Racanelli, 2017). Additional to this, it is cytoprotective, as it removes invading bacteria and viruses (Kuwano, 2016). As mentioned previously, it is a constitutive process with a baseline activity. However, if cells are exposed to cellular stress, the activity level increases. Depending on the type of inducer, different subtypes of autophagy are activated (Levine & Kroemer, 2008; Racanelli, 2017).

These subclasses are denoted as macroautophagy, microautophagy and chaperone-mediated autophagy (Cao, 2021; Glick et al., 2010; Racanelli, 2017). Macroautophagy transfers intracellular cargo, via autophagosomes which are ultimately delivered to the lysosomal compartment for degradation. Microautophagy involves direct uptake of intracellular components into the lysosome through a membrane-invagination mechanism, while chaperone-mediated autophagy involves specific targeting of proteins and their translocation across the lysosomal membrane by the aid of chaperone proteins (Glick et al., 2010; Kocak, 2021). Additionally, autophagy can be divided into subgroups based on the cargo. For example, mitophagy refers to the maintenance and degradation of damaged mitochondria while xenophagy involves removal of intracellular bacteria and viruses (Cao, 2021). The focus of this thesis is macro-autophagy and it will hereon be referred to as only 'autophagy'.

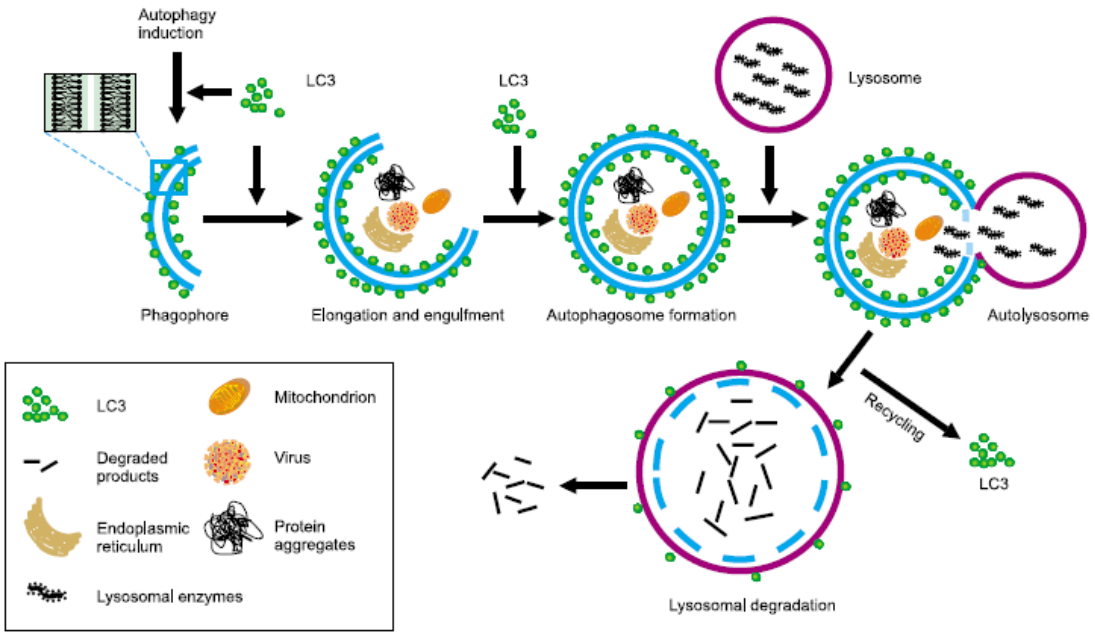

Figure 1. A schematic overview of the autophagy process (Ling et. al., 2012). *The scheme shows how the phagophore develops into an autophagosome and during this maturation process ingulfs protein aggregates, viruses, damaged mitochondria och endoplasmic reticulum. It also incorporates LC3-proteins into its inner and outer membrane. Next, the autophagosome fuses with a lysosome, thereby transforming into a autolysosome. In this step, the LC3 becomes recycled and the lysosomal content degraded by lysosomal enzynes.*

The molecular mechanism of autophagy

The autophagy process occurs in the cytoplasm and can be divided into different stages: 1) initiation, 2) isolation of membrane/the so called phagophore, 3) membrane elongation with incorporation of membrane-bound microtubule-associated protein 1A/1B-light chain 3 (LC3), 4) phagophore closure and subsequent autophagosome formation, and lastly 5) autophagosome fusion with a lysosome, followed by acidification and autolysosomal degradation of cargo (Glick et al., 2010; Nishimura, 2020). The initiation signal can be nutrient deficiency or cellular damage due to e.g. oxidative stress caused by smoke inhalation. The following sections provide a detailed description of the different stages of autophagy. The sum of these different stages is also referred to as autophagy flux (Zhang, 2013).

The best characterized mechanism for autophagy induction is amino acid starvation. This process is governed by the mammalian target of rapamycin (mTOR) pathway. The mTOR is a kinase which senses and regulates cell growth in response to different cell signals, e.g. starvation (Blenis, 2017; Wullschleger et al., 2006). The mTOR kinase can be found in two different complexes, the mammalian target of rapamycin complex 1 (mTORC1) and the mammalian target of rapamycin complex 2 (mTORC2), in which mTORC1 is of relevance to this thesis. This because mTORC1 is responsible for cell growth and upon activation, blocks autophagy. The mTORC2 on the other hand, is involved in the regulation of cytoskeleton growth (Wullschleger et al., 2006). As mTORC1 is activated, it prevents autophagy and stimulates processes such as ribosome biogenesis, translation, and nutrient import. Hence, this occurs in nutrient-rich conditions (Kim et al., 2011; Wullschleger et al., 2006). However, during starvation, mTORC1 is inhibited due to a lack of amino acids and mitogen signalling, and by inhibition via AMP-activated protein kinase (AMPK).

AMPK is a kinase which senses the energy level of the cell, i.e the AMP/ATP ratio. AMPK is activated by low cellular energy (high AMP/ATP ratio) and upon activation, phosphorylates tuberous sclerosis complex 2 (TSC2). This leads to mTORC1 inhibition (Kim et al., 2011; Wullschleger et al., 2006). Another important complex is the Ulk1 complex, regulated by AMPK. As AMPK phosphorylates two serine sites in Ulk1 (Ser317, Ser777), autophagy is induced. Ulk1 is a part of the Ulk1-mAtg13-FIP200 complex in mammals, a key complex for autophagy initiation autophagy (Kim et al., 2011). During nutrient rich conditions is this complex suppressed by mTORC1 through inhibitory phosphorylation (Zachari & Ganley, 2017). Therefore, during starvation conditions when mTORC1 is inhibited, the Ulk1 complex is active and can take part in the induction of autophagy.

As the Ulk1 complex is activated, it translocates to the autophagy initiation site close to the endoplasmic reticulum (ER) and recruits a second complex, the Vps34 complex. The Vsp34 complex consists of class III phosphatidylinositol 3-kinase Vps34, beclin-1 and Atg14L. The complex produces phospholipid phosphatidylinositol 3-phosphate (PI3P), which acts as a signalling molecule for other proteins in the autophagy process (Zachari & Ganley, 2017). The Ulk1 complex and the Vsp34 complex are, together with other proteins, essential for the initiation of the phagophore formation.

Following the initiation and formation of the phagophore, the phagophore membranes expand and cytosolic LC3B (LC3-I) is converted into a phosphatidylethanolamine (PE) conjugated form (LC3II). This form is incorporated into the inner and outer phagophore membranes. Briefly, pro-LC3B is cleaved by the cysteine protease Atg4, thereby forming cytosolic LC3-I. Subsequently, LC3-I is activated by Atg7 and transferred to Atg3. Next, PE is conjugated to LC3-I, thereby forming LC3-II. Lastly, the Atg5-Atg12-Atg16 complex directs the incorporation of LC3-II into the maturing phagophore (Glick et al., 2010; Kawabata & Yoshimori, 2020). LC3-II is involved in several steps of the autophagy process: autophagosome closure, movement of the autophagosome, fusion with the lysosome and the degradation of the inner membrane of the autophagosomes (Kawabata & Yoshimori, 2020). Because of its localization in the phagophore/autophagosome membrane, it is also a well-used marker for measuring autophagy flux.

As the phagophore matures, intracellular cargo becomes ingulfed, including proteins and organelles. LC3-II interacts with another autophagy marker, p62/SQSTM1. The p62 is an

adaptor protein which binds ubiquitinated proteins and upon interaction with LC3-II, ensures incorporation of these proteins and itself into the maturing phagophore (Glick et al., 2010; Pankiv et al., 2007). Since p62 is degraded through the autophagy process, it is a common marker for the measurement of autophagy flux.

Upon fusion of the phagophore ends, the autophagosome formation is complete. Studies suggest that the autophagosomes migrate towards the perinuclear area in the cell, where the lysosomes can be found (Kawabata & Yoshimori, 2020). Subsequently, as the autophagosome fuses with a lysosome, it forms an autolysosome. This process is regulated by EPG5 and INPP5E, driving for example the formation of the SNARE-complexes (Kawabata & Yoshimori, 2020). After fusion and lysosomal acidification, the cargo carried by the autophagosome becomes degraded by the lysosomal enzymes (Glick et al., 2010). Hence, this leads to the recycling of amino acids and other macromolecules such as lipid and carbohydrates, thereby enabling the cell to survive during starvation conditions. Furthermore, the autophagy process allows for the recycling of damaged proteins and organelles, which is expected to rise in the setting of cell stress.

Senescence

Senescence is a process characterized by irreversible cellular growth arrest, resistance to apoptosis and the SASP. Apart from being correlated with aging, the disease has been connected to multiple diseases including COPD (Hamsanathan et al., 2019; Muñoz-Espín & Serrano, 2014). The main risk factors for senescence are increasing age, mitochondrial dysfunction and environmental exposures that promote senescence (Hamsanathan et al., 2019).

Senescent cells have a different profile in terms of signalling molecules, chromatin organization and gene expression. Furthermore, are senescent cells cleared by immune cells which in turn has been recruited by SASP signalling molecules (Hamsanathan et al., 2019).

The SASP is a pro-inflammatory but complex secretory profile, varying between different cell types and tissues. However, the SASP has shown to include expression of multiple cytokines, e.g. IL-6 and IL-8 and other cytokines from the interleukin protein family. Furthermore, the SASP includes expression of different specific chemokines, growth factors and proteases. The protease expression drives the remodelling of the extracellular matrix (ECM). Additionally, the SASP has been shown to include formation of microvesicles, which are important for intercell communication and for the transfer of components such as mRNAs, proteins and microRNAs between cells (Hamsanathan et al., 2019; Kuwano, 2016; Muñoz-Espín & Serrano, 2014).

There are multiple senescence-associated markers and characteristics for a senescent cell. Altered morphology, increased levels of cell cycle regulators, condensed chromatin regions and the senescence-associated β-galatosidase (SA-β-Gal) are all used as markers. However, there are no golden standard for the identification of senescent cells since the markers can vary between cells and tissues. Hence, using multiple markers is currently the most robust way to identify senescent cells (Hamsanathan et al., 2019; Kuwano, 2016; Muñoz-Espín & Serrano, 2014).

As mentioned previously, senescence can be divided into two subtypes, based upon on the inducer. Firstly, telomere-dependent replicative senescence and secondly, stress-induced senescence. Telomere-dependent replicative senescence involves the loss of telomere sequence

due to the many cell divisions a cell goes through during its lifetime. At a certain point, the telomeres have been shortened to such a degree that the cell does into replicative senescence (Kuilman et al., 2010; Wang et al., 2009). Stress-induced senescence derives from stress signals and exposures, e.g. oxidative stress. They give rise to increased DNA-damage and mitochondrial dysfunction which in turn can lead to senescence (Hamsanathan et al., 2019).

The molecular mechanism of senescence

Senescence-induced growth arrest can occur through two main pathways: the p53/p21 pathway and the p16 pathway, in which only the first pathway will be accounted for here (Hamsanathan et al., 2019; Muñoz-Espín & Serrano, 2014). As there are multiple different types of inducers, there are also several initiation pathways.

In the case of oxidative stress, the increase in ROS increases the activity of the p38 MAPK. This leads to increased expression of p53. Subsequently, the p53 induces expression of p21, a cyclin-dependent cell cycle inhibitor. The p21 goes on to inhibit cyclins D and E in the nucleus, which leads to the activation of the retinoblastoma protein pRb. The action of pRb prevents the cell form entering the S phase, by the inhibition of transcription factor E2F, leading to cell cycle arrest (Hamsanathan et al., 2019; Muñoz-Espín & Serrano, 2014).

As stated previously, the SASP involves a proinflammatory response, resulting in increased secretion of pro-inflammatory cytokines interleukin-6 (IL-6) and interleukin-8 (IL-8). Additional to this, the expression and secretion of chemokines such as MCP-1, -2, -3 and -4 (monocyte chemoattractant proteins), HCC-3, eotaxin 3 and MIP-1a and -3a (macrophage inflammatory proteins) increase, together with levels of macrophage inflammatory proteins (MIPs), growth factors and proteases. Apart from increasing inflammation, does these signalling molecules recruit immune cells for the phagocytosis of senescent cells (Hamsanathan et al., 2019; Muñoz-Espín & Serrano, 2014).

The connection between autophagy and senescence in COPD

In the context of COPD, studies have shown that autophagy is affected in diseased patients. In fact, autophagy is impaired in COPD patients, resulting in accumulation of proteins, and so called aggresome bodies. Furthermore, impairment of autophagy correlates with increased senescence-associated markers in these cells (Fujii et al., 2012; Kuwano, 2016; Vij et al., 2016).

Aim of the project

With this background, the aim of this project was to study whether primary human bronchial epithelial cells (HBECs) and primary human lung fibroblasts (HLFs) from COPD and healthy donors exhibit impaired autophagy and increased senescence-associated markers upon exposure of cigarette smoke extract (CSE). The decision to use CSE was based upon that the main risk factor for COPD is smoking (Matsunaga et al., 2020; Racanelli, 2017).

Specifically, we wanted to determine which cell type is most affected by CSE as well as investigate the response in the context of autophagy and senescence. Additionally, was it relevant to elucidate which cell type could be most appropriate for an *in vitro* COPD cell model, with the purpose of modulating autophagy and senescence. Investigation into the most relevant model for this type of studies could aid the field and improve future research. Furthermore,

could a comparison between the response in different cell types provide additional knowledge and insights.

The aims were met by studying multiple markers for autophagy and senescence, using immunocytochemistry and immunoblotting techniques. By looking at autophagy markers, in this case p62 and LC3, we could better understand if and how autophagy was affected and altered following CSE treatment, in COPD patients and controls. The investigation into senescence-associated markers p21 and SA-β-Gal in cells from the same patients, could provide further information about the level of senescence in these cells.

Materials and Methods

Cell cultures and cell seeding

HBECs and NHLFs were used in the project. For the NHLFs, two experiments were run using the same healthy donor (lot 655309). For the HBECs, one experiment with one healthy donor and one COPD donor was performed (healthy donor N3375; diseased donor D0389). Cells were provided as frozen aliquots of 500 000 cells/vial from Lonza in passage 3.

After thawing, the cells were incubated in T175 or T75 cell culture flasks at 37℃ in 15mL of appropriate media. Following media was used: bronchial epithelial cell growth basal medium 1X (BEGM; Lonza) for HBECs, Dulbecco's modified eagle medium 1X (DMEM; Gibco) + GlutaMAX-1 (Gibco) for NHLFs. The NHLFs were seeded and incubated for 48h without media change, while the HBECs were seeded and grown for one week, with media change every second day. When reached cell confluence of 70-80%, the cells were plated in 96-well black-walled PhenoPlates (Perkin Elmer) and 12-well CoStar plates (Corning). Cell seeding density was 4000 cells/well for the NHLFs. For the HBECs, cell density was adjusted for each time point to prevent cells from overgrowing at the later time points (see table 1, p. 8). Cell viability was above 90% in all experiments. Following seeding, the plates were incubated for 24h at 37℃ and 5% CO_2 before addition of treatments.

Table 1. HBECs seeding numbers for the different time points, donors and plates. *These time points were not plated due to too low cell count.

	Healthy donor		**COPD donor**	
	96-well	**12-well**	**96-well**	**12-well**
5h time point	16 000 cells/well	300 000 cells/well	16 000 cells/well	200 000 cells/well
24h time point	16 000 cells/well	300 000 cells/well	16 000 cells/well	200 000 cells/well
48h time point	10 000 cells/well	200 000 cells/well	X*	150 000 cells/well
72h time point	8 000 cells/well	150 000 cells/well	X*	100 000 cells/well

Treatments

The cells were treated with increasing concentrations of cigarette smoke extract (CSE) and subsequently harvested at different time points (see table 2, p. 9). Multiple controls were used for each experiment (table 2, p. 9). The CSE was prepared and diluted in 1X Dulbecco's phosphate-buffered saline (DPBS; Gibco).

Cigarette smoke extract (CSE) preparation

For the preparation of 100% CSE, 5 2R4F Kentucky research cigarettes (University of Kentucky, Kentucky Tobacco Research and Development Center) were bubbled through a glass flask containing 25mL of DPBS (Gibco), where the smoke was solubilized. Air flow was adjusted to 0.07 L/min and it took 5 minutes to smoke one cigarette. Following smoking, CSE was filtered through 0.22 µm filters and subsequently aliquoted and frozen immediately on dry ice, stored at -80°C.

Table 2. The CSE concentrations and time points used for experiments with HBECs and NHLFs, including control substances and number of experimental repeats.

	HBECs	**NHLFs**
Concentrations of CSE for each time point (%)	0 0.5 1 3	0 0.15625 0.3125 1.25 2.5 5 10 20
Time points of cell harvest	5h 24h 48h 72h	6h 24h 48h 72h
Control substances	Bafilomycin 100nM, 3h DMSO (bafilomycin control), 3h Etoposide 3µM, 72h DMSO (etoposide control), 72h Torin 50nM, 3h	Bafilomycin 100nM, 3h DMSO (bafilomycin control), 3h Etoposide 3µM, 72h DMSO (etoposide control), 72h Torin 50nM, 3h
Number of experimental repeats	0	1

Immunocytochemistry

Following treatments with CSE and control substances, the 96-well plates were fixed using already prepared 4% paraformaldehyde (PFA) in phosphate buffered saline (PBS; Thermo Scientific Chemicals) for 10 minutes. Following three washes with DPBS (Gibco), cells were stored in DPBS at 4℃.

Subsequently, the cells were permeabilized with 100µL of 0.2% Triton-X in DPBS for 10 minutes at room temperature. After three washes in DPBS, the cells were blocked in Super Block (DAKO, 37580) for 60 minutes on rocking platform at room temperature. The cells were then incubated with primary antibodies in antibody diluent (DAKO, S3022). Primary antibodies used were anti-LC3 (dilution 1:200; incubation overnight at 4 ℃; Cell Signalling Technology, #2775), anti-p62/SQSTM1 (dilution 1:200; incubation 1.5h at room temperature; Cell Signalling Technology, #5114). Following incubation, each well was rinsed with 100µL of 0.5% Tween-20 in DPBS for 5 minutes. Subsequently, the cells were incubated with secondary antibodies (Alexa Fluor™ 488, Alexa Fluor™ 568; Invitrogen) in antibody diluent (DAKO, S3022) for 1h. Following one wash with 0.05% Tween-20 in DPBS and three washes with DPBS, cells were kept in 200µL of DPBS and stored at 4℃ until imaging using Yokogawa CV7000/CV8000. These are high content screening systems (HCA) with a confocal scanner, which enables fluorescence-based cell imaging (Yokogawa, 2023).

Columbus™ analysis scripts

The Columbus™ software (PerkinElmer) can be used to analyse images taken in e.g. the Yokogawa. Using this software, the signal intensity of the fluorescent antibodies can be quantified and measured, as well as determination of e.g. cell count.

For p62 intensity, the script was as follows: a) find nuclei (method C), b) find cytoplasm (method B), c) selection of no border population, d) calculate intensity properties of the no border cell population and with the cytoplasm as region. The standard method was used, giving total intensity of each well. This intensity was subsequently divided by number of nuclei in the specific well, giving p62 intensity/cell. This was done for each time point using the batch analysis tool.

To measure SA-β-Gal intensity and p21 intensity, the same script was used. However, for the finding nuclei step, method B was used instead.

LC3II-puncta were manually quantified in Columbus™ due to high cytoplasmic background and difficulty to differentiate spots with the Columbus™ scripts. For each time point, the puncta in 50 cells were counted manually from the images. However, the 48h and 72h time points could not be quantified due to a high number of fused puncta.

Protein extraction and quantification for immunoblotting

The 12-well plates were used for cell seeding for immunoblotting. Whole cell proteins were extracted and quantified using a bicinchoninic acid (BCA) assay (details further down). Proteins LC3, p62 and p21 were of interest.

Following treatments, the wells were washed with 500µL of ice-cold DPBS (Gibco), followed by addition of 85µL of lysis buffer (RIPA buffer, phosphatase inhibitor cocktail 1:100, protease inhibitor cocktail 1:100; Thermo Fisher). Subsequently, the cells were detached using plastic

scrapers and incubated on ice for 5 minutes with repeated shaking. Following this, cells were transferred to Eppendorf tubes and incubated on ice for approximately 30 minutes. After incubation, the samples were centrifuged at 13K rpm for 10 minutes at 4℃. Lastly, the supernatant was collected into new Eppendorf tubes and stored at -80℃.

Next, the protein concentration of each sample was determined using the Pierce™ BCA protein assay kit (Thermo Fisher) according to manufacturer's instructions. Standards were previously prepared and stored at -20℃, and absorbance was measured at 562 nm.

Immunoblotting

To prepare proteins for denaturing gel electrophoresis, NuPAGE™ 1X LDS sample buffer (Thermo Fisher) was added to each sample. The samples were subsequently denatured at 95℃ for 5 minutes. Samples were then resolved using NuPAGE™ 10 and/or 12-well gels (Thermo Fisher), using the XCell SureLock Mini-Cell gel tanks and 1X MOPS buffer. The gels were run for approximately 1.5h at 120V. Subsequently, semi-dry transfer kits (BioRad) were used for transferring the proteins in the gel to a polyvinylidene fluoride (PVDF) membrane using the BioRad Trans-Blot Turbo Transfer System. After transfer, the membranes were marked and cut, with the LC3 bands on one membrane and the p62 and GAPDH bands on a second. This because the primary antibodies for LC3 and p62 were both generated in mouse. Hence, the secondary antibody would cross-react to both protein bands if mixed. The different membranes were blocked in Li-Cor blocking buffer for 1h shaking at room temperature. The membranes were incubated with the appropriate primary antibody in Li-Cor blocking buffer overnight, rotating in the tubes at 4℃. The following antibodies were used: anti-LC3 (1:2000 dilution, Abcam ab192890), anti-p62 (1:2000, Abcam ab109012), anti-GAPDH (1:10 000, Cell Signalling technology). The next day, the membranes were washed in tris-buffered saline + Tween-20 (TBST) 3x 15 minutes each and incubated with secondary antibodies (goat anti-mouse, goat anti-rabbit; Li-COR) in Li-Cor blocking buffer for 2h. Following three washes in TBST, the membranes were imaged using Li-Cor Odyssey CLx. From the Li-Cor images, the protein density units were measured using ImageStudio software (Li-Cor), based on the fluorescent signal and then normalized to glyceraldehyde 3-phosphate dehydrogenase (GAPDH).

Statistical analysis

The data was plotted in GraphPad Prism 9 and all the statistical analysis was done within this programme. For the immunocytochemistry data, an ordinary one-way ANOVA was performed for each plotted time point and with at least three replicates for each sample. A multiple comparison was also performed for each time point, in which each sample was compared to the control sample for the time point. The samples with significant difference to the control sample, i.e significant p-value, are shown in the plots found in the figures (fig. 2-5, p. 14-20).

For the immunoblotting, there are only one replicate for each sample from each donor. Hence, no satisfactory statistical analysis could be performed.

Results

The follow results are for the HBECs unless stated otherwise.

HBECs from one healthy and one COPD donor were exposed to different concentrations of CSE in order to study the cell response, with focus on autophagy and senescence. LC3-II and p62 were the autophagy markers used, and p21 and SA-β-Gal for senescence. The aim was to see whether the autophagy markers would increase in response to CSE and if we could observe impaired autophagy, i.e accumulation of both markers. Furthermore, we were interested to observe the levels of the senescence-associated markers and if they would increase in response to CSE. We also wanted to investigate if we could find a connection between impaired autophagy and increased senescence-associated markers.

Autophagy: immunoblotting

The cells were exposed to different concentrations of CSE (0%, 0.5%, 1% and 3%) for different durations: 5h, 24h, 48h and 72h. At the 5h time point, the immunoblot shows an accumulation of p62 for both the healthy and COPD donor (fig 2a, p. 13). The increase is expressed as the ratio of p62 to GAPDH, which is a housekeeping gene commonly used as comparative marker in immunoblotting. With the ratios normalized to the control sample (0% CSE) within each donor, the data shows a stronger response in the healthy donor compared to the COPD donor. However, with both donors normalized to the healthy donor's control sample, the data suggests that the COPD donor has a higher baseline signal of p62 compared to the healthy donor (fig 2a, p. 13).

The LC3-II signal increases in both donors at the 5h time point (fig 2a, p. 13). It is slightly different when comparing them, in that the healthy donor has a strong increase of LC3-II signal at 3% CSE while the COPD donor shows a sequential increase (fig 2a, p. 13). When the signals are normalized to the same control (healthy donor, 0% CSE), the data is more or less the same as for the normalization within each donor (fig 2a, p. 13).

At the 24h time point, the western blot shows a sequential increase of p62 in both donors (fig 2b, p. 13). For LC3-II, the increase is evident at the 3% CSE concentration, in both donors (fig 2b, p. 13).

In the two later time points, 48h and 72h, the pattern for p62 and LC3-II are similar. Here, the main increase of p62 signal occurs at 3% CSE in both donors (fig 2c; fig 2d, p. 13). Important to note, is that the 3% CSE sample from the COPD donor is missing at the 72h time point. This due to too low protein concentration in that sample.

For LC3-II, the healthy donor shows a decreased signal at the lower concentrations of CSE at both time points. However, in the 3% CSE sample at the 72h time point, there is a strong increase in LC3-II in the healthy donor (fig 2c; fig 2d, p. 13).

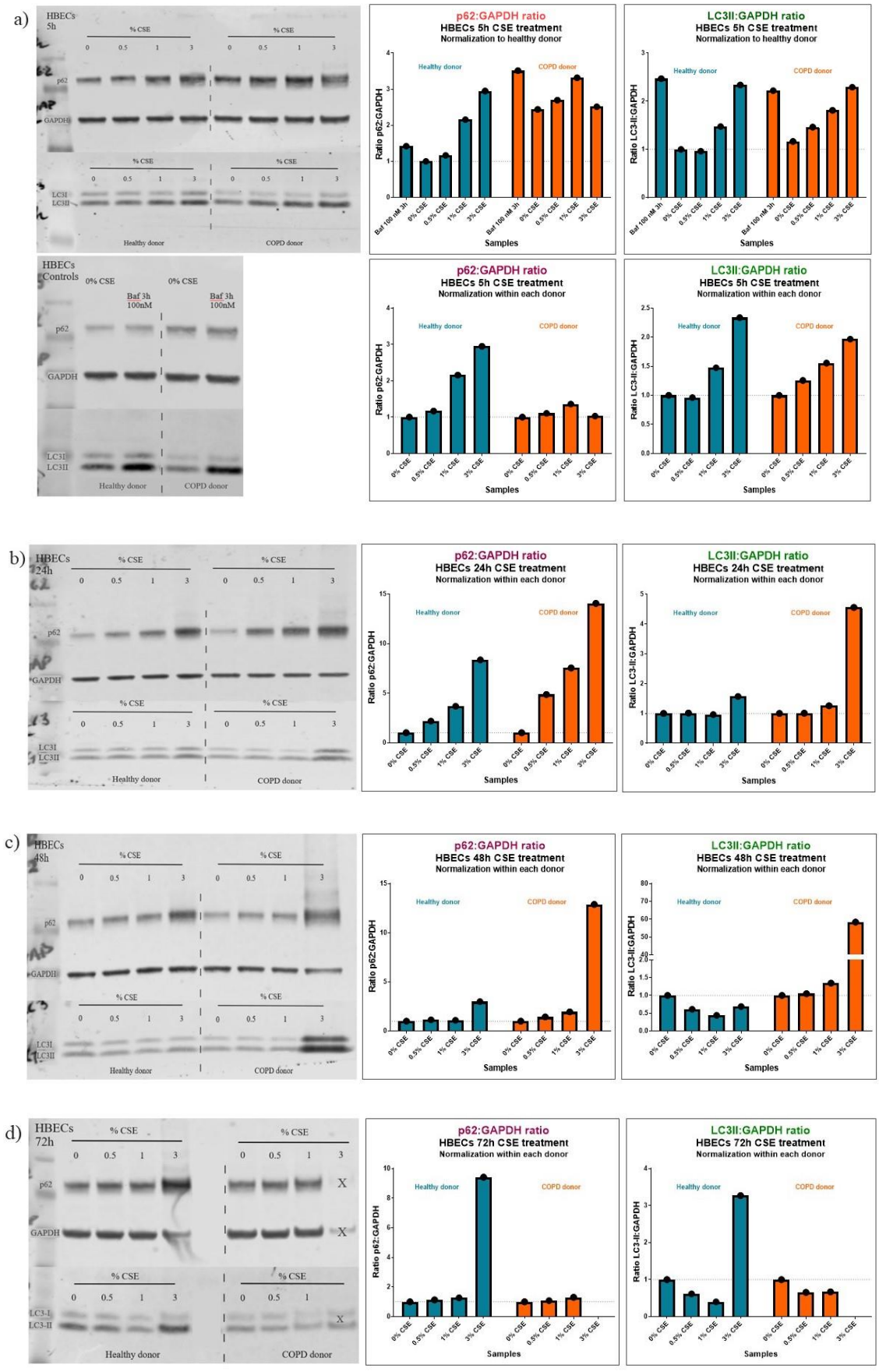

Figure 2. The immunoblotting data of the autophagy markers p62 and LC3 for the different CSE concentrations at the different time points in HBECs. *To the left shows the western blot gel, with p62, LC3 and the marker protein GAPDH for*

each sample. In each gel can the healthy donor be found on the left, and the COPD donor on the right. To the right in the figure, are the graphs showing the quantified signals of the protein bands. The quantification is showed in ratios, comparing the protein of interest (p62 or LC3-II) normalized to the GAPDH band in each sample. The healthy donor is shown in blue and the COPD donor in orange. All time points are included in the figure: a) 5h, b) 24h, c) 48h, and d) 72h, and refers to the duration of CSE incubation. For a) the sample signals have been normalized to both the healthy donor (top) and within each donor (bottom). B) to d) show only normalization within each donor. The experiments were run once for each donor, with no replicates.

Autophagy: immunocytochemistry

The immunocytochemistry data, available for only the 5h and 24h time points, supports the immunoblotting data to a high degree (fig 3a, p. 14). The exceptions are as follows: firstly, the 5h 3% CSE sample for the COPD donor show a stronger signal than the healthy donor's, which is contrary to the immunoblotting data (fig 3a, p. 14). Secondly, the same type of contradiction can be found at the 24h time point, for the LC3-II 3% CSE samples. Here, the signal is stronger in the healthy donor, which is opposite to the results from the immunoblotting (fig 3b, p. 15).

Autophagy: the control substance bafilomycin

Bafilomycin was used as a control for autophagy, as it is a well-known autophagy inhibitor. A 3h exposure of 100nM bafilomycin gives rise to a slight increase in p62 in both donors in the immunoblotting data (fig 2a, p. 13). This increase is supported in the immunocytochemistry data (fig 3a, p. 14). Regarding LC3-II, the increase is strong in both donors in the results from the immunoblotting (fig 2a, p. 13). In the immunocytochemistry though, the increase is not as strong (fig 3a, p. 14).

Autophagy: summary of results

Conclusively, the autophagy data shows increased expression of p62 and LC3-II in the two early time points (5h and 24h) for both donors, with the baseline autophagy activity being higher in the COPD donor than the healthy at the 5h time point. Hence, the data suggests an impaired autophagy flux at these time points.

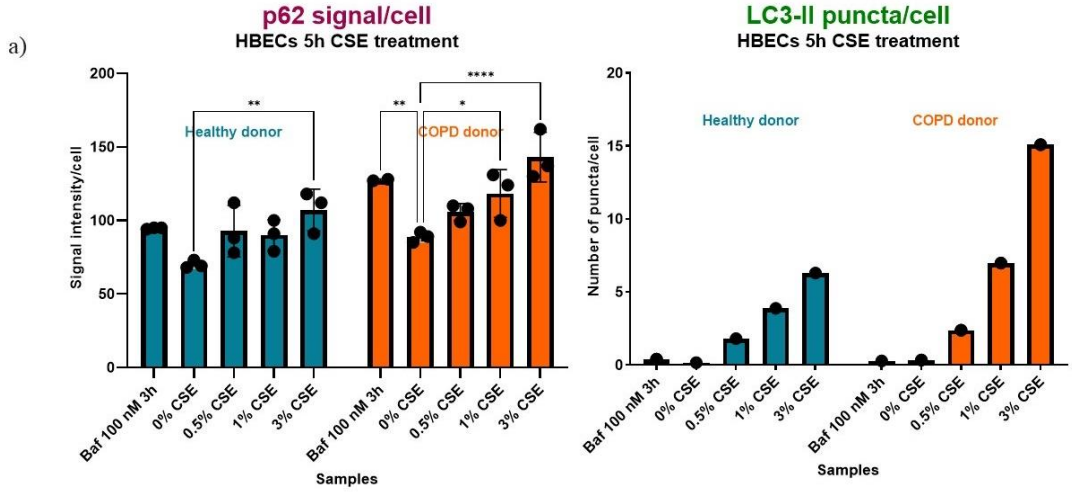

b)

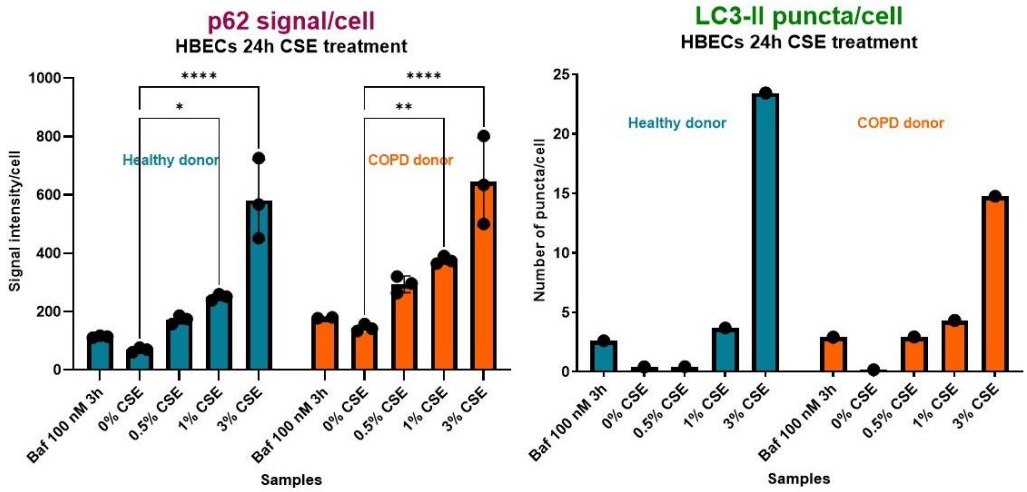
p62 signal/cell
HBECs 24h CSE treatment
Signal intensity/cell
Healthy donor
COPD donor
Baf 100 nM 3h
0% CSE
0.5% CSE
1% CSE
3% CSE
Samples
LC3-II puncta/cell
HBECs 24h CSE treatment
Number of puncta/cell
Healthy donor
COPD donor
Samples

c)

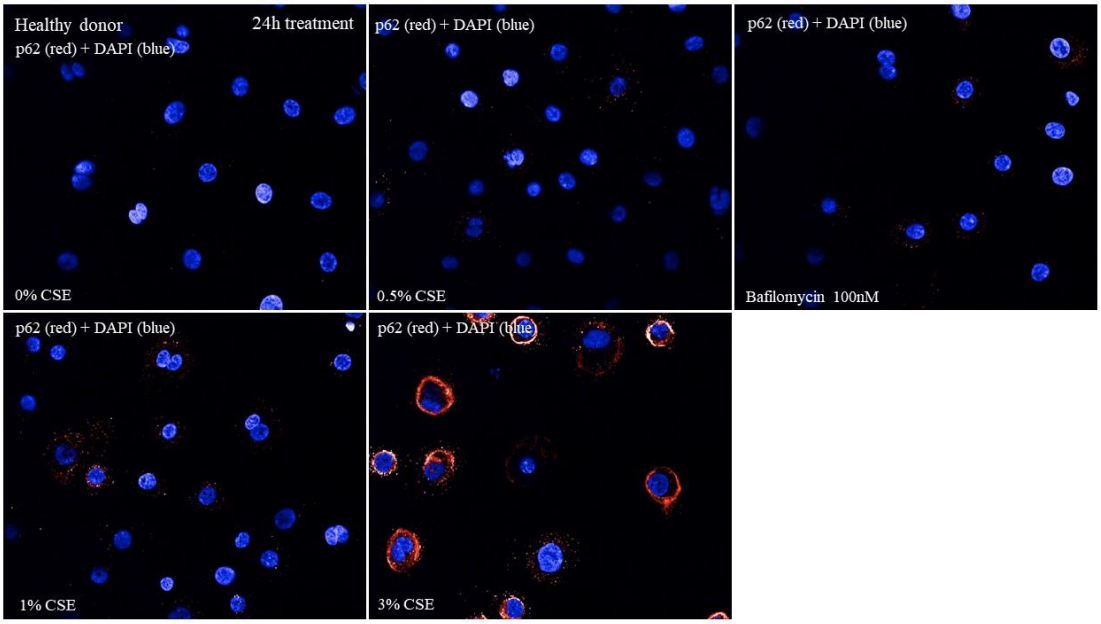
Healthy donor
24h treatment
p62 (red) + DAPI (blue)
0% CSE
0.5% CSE
Bafilomycin 100nM
1% CSE
3% CSE

d)

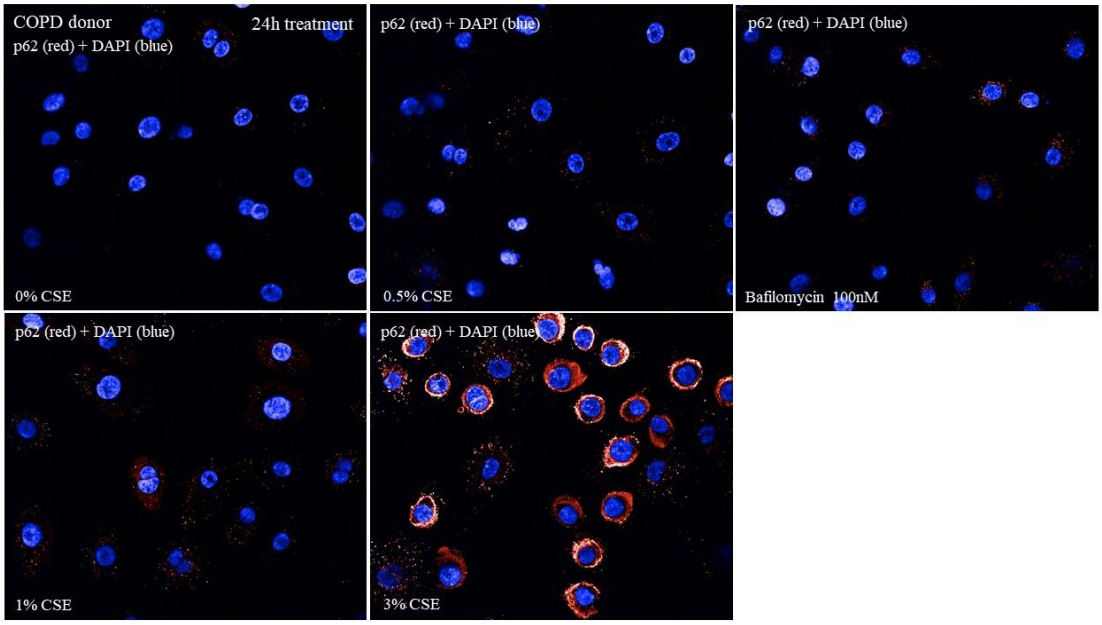
COPD donor
24h treatment
p62 (red) + DAPI (blue)
0% CSE
0.5% CSE
Bafilomycin 100nM
1% CSE
3% CSE

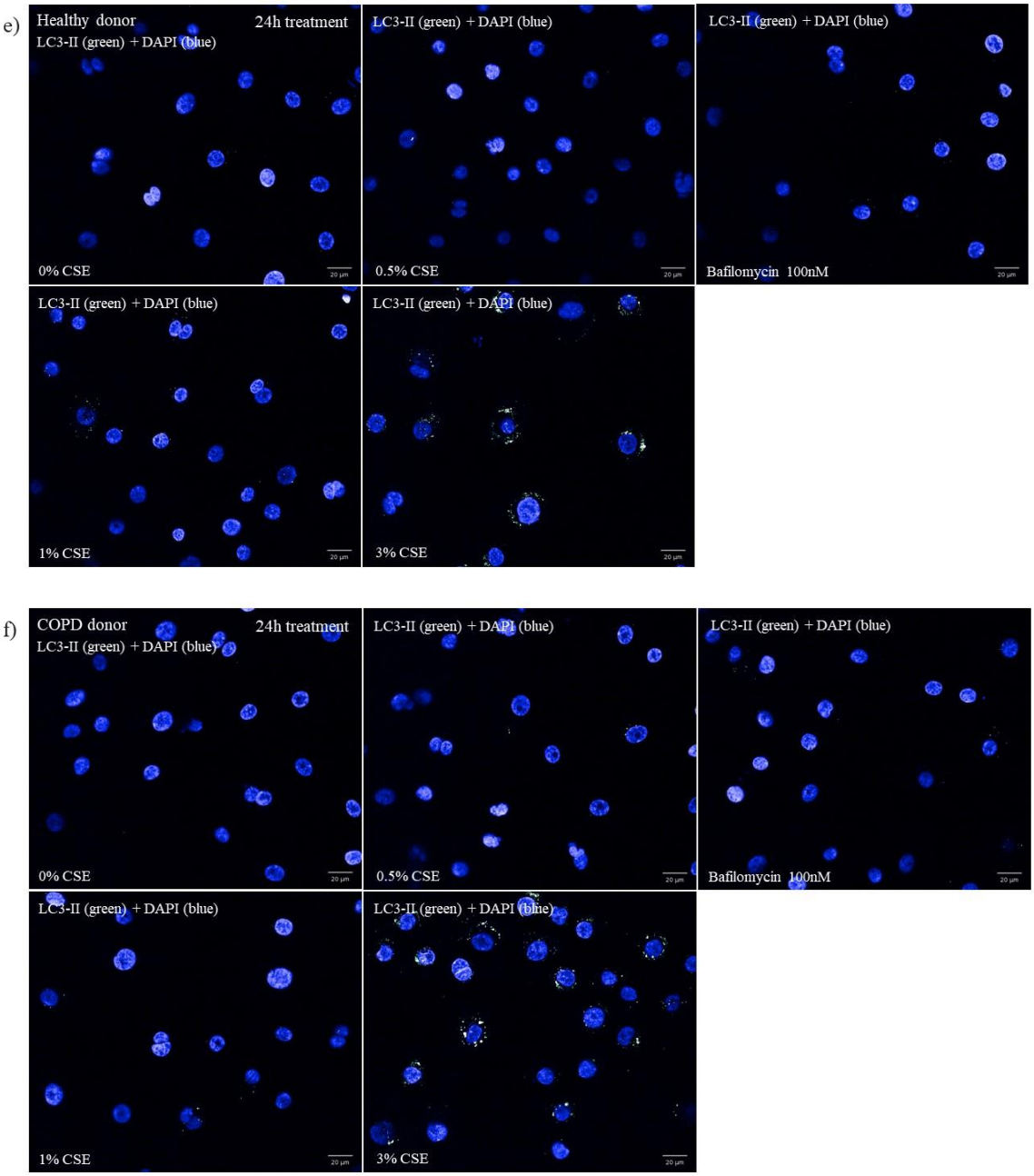

Figure 3. The immunocytochemistry data for the HBECs and the autophagy markers p62 and LC3-II, for each time point. *a) and b) shows the quantified and subsequently plotted signals of p62 and LC3-II, in which p62 signal is given in signal/cell while LC3-II is given in puncta/cell. The p62 signals are quantified using a Columbus batch analysis script while the LC3-II puncta are derived from manual estimation of puncta on the Yokogawa images. A) shows the plot for the 5h time point and b) for the 24h time point. c)-f) show the Yokogawa images for the 24h time point for both healthy and COPD donor, as an example. c) and d) are the p62 and LC3-II stained cells from the healthy donor, respectively. e) and f) show instead for the COPD donor. The nucleus is shown in blue, the p62 protein in red and the LC3-II protein in green. The experiments were run once for each donor, with triplicates for each sample. Error bars in the graphs represent the SEM.*

Senescence

Senescence was determined using immunocytochemistry for two senescence-associated markers: SA-β-Gal and p21. Firstly, the SA-β-Gal experiments show an increase in SA-β-Gal signal correlating with increasing CSE concentration (fig 4a-c, p. 17). The increase is significant for 3% CSE for all three time points (24h, 48h and 72h).

These findings are partly supported by the data for the p21 protein marker (fig 5a-c, p. 19). For the 24h time point, the increase of nuclear p21 is evident and significant – for both healthy donor and COPD donor. However, for the later time points, is the increase not as strong. Compared to the 0% CSE control there is an increase, however, it does not differ much between the CSE concentrations.

Noteworthy is that we do not have data for 48h and 72h for the COPD donor, due to too low cell count when seeding.

In terms of cell death and nuclear size (fig 6, p. 20), the number of cells decrease with increasing CSE concentration. Furthermore, is the nuclear size of the cells changing. The nucleus size increases with rising CSE concentration, until 3% CSE when it drops drastically (fig 6d-f, p. 20). In exception, at the 24h time point does the healthy donor show a decrease in nucleus size for all CSE concentrations.

Senescence: the etoposide control

The etoposide control shows an increase in SA-β-Gal after 72h etoposide incubation, although, the signal is not as strong as for the CSE exposures (fig 4c, p. 17). Regarding p21, there is an increased signal in the etoposide control after 72h incubation (fig 5c, p. 19). However, it is not significant and not as strong as for the CSE exposed samples.

Senescence: summary of results

To conclude the senescence part, the data show increased senescence-associated markers after CSE exposure. However, the p21 and SA-β-Gal data do not fully correspond for the two later time points (48h and 72h). For the 24h time point, both markers are increased after CSE exposure, mainly at the 3% CSE concentration.

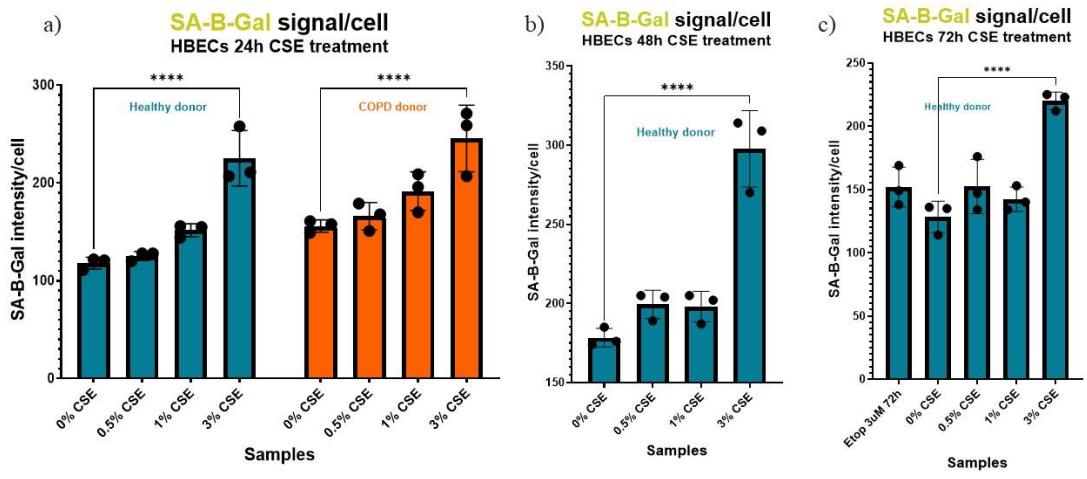

d)

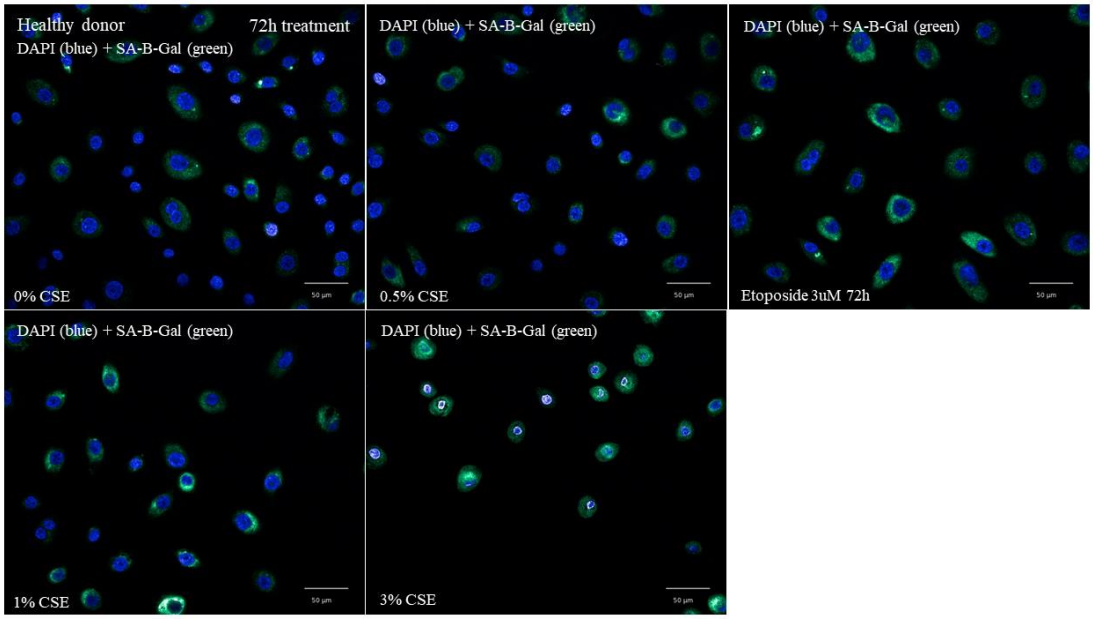

Figure 4. The immunocytochemistry of the SA-β-Gal staining of healthy and COPD donor for the 24h, 48h and 72h time points in HBECs. *The quantified signals of SA-β-Gal are shown in a) 24h, b) 48h and c) 72h. Figure d) includes the Yokogawa images of the staining for the 72h time point, shown as an example. The nucleus can be seen in blue while the SA-β-Gal protein is in green. The experiments were run once for each donor, with triplicates for each sample. Error bars in the graphs represent the SEM.*

NHLFs

Despite running the same protocols and methods for the NHLFs, the results were inconclusive. Experiments were only run on one healthy donor. The immunoblotting and immunocytochemistry for p62 were detectable and would have been able to analyse, however the LC3-II signal in the immunocytochemistry was not detectable. Furthermore, the LC3-II pattern in the immunoblotting was unexpected and would have needed further investigation to determine whether it was the actual case, if it was donor-dependent or if it was an experimental artifact of some kind. We therefore decided not to proceed with these experiments and therefore, no data for these cells are presented in the main thesis. For data, see Appendix (p. 27-29).

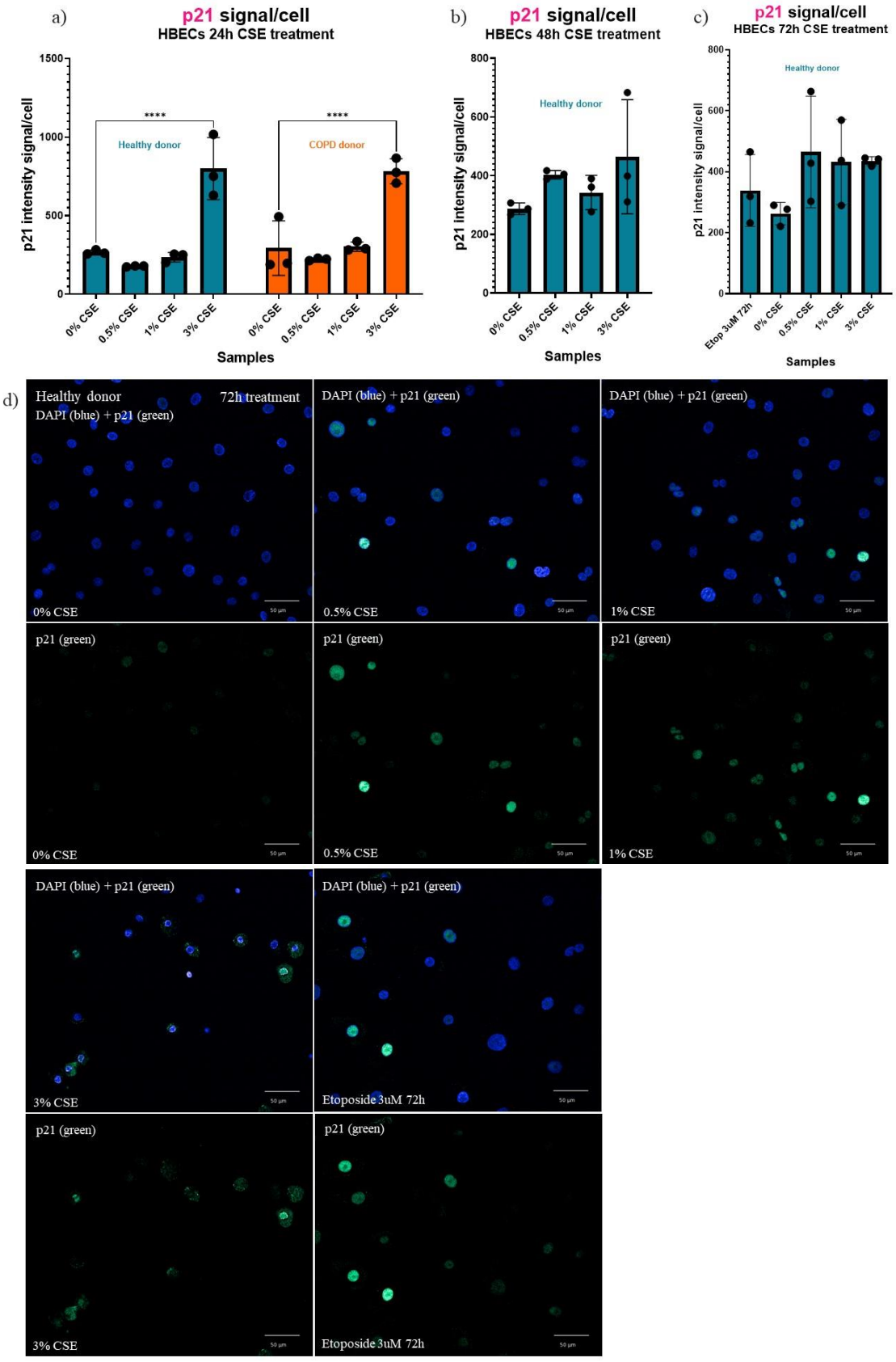

Figure 5. The immunocytochemistry of the HBECs stained with p21 antibody*. A)-c) shows the Columbus quantified signal of p21 signal/cell for the a) 24h, b) 48h and c) 72h. d) shows the Yokogawa images in which the quantification is based upon, with the 72h time point as an example here. The p21 staining is green while the blue refers to nuclear staining. The experiments were run once for each donor, with triplicates for each sample. Error bars in the graphs represent the SEM.*

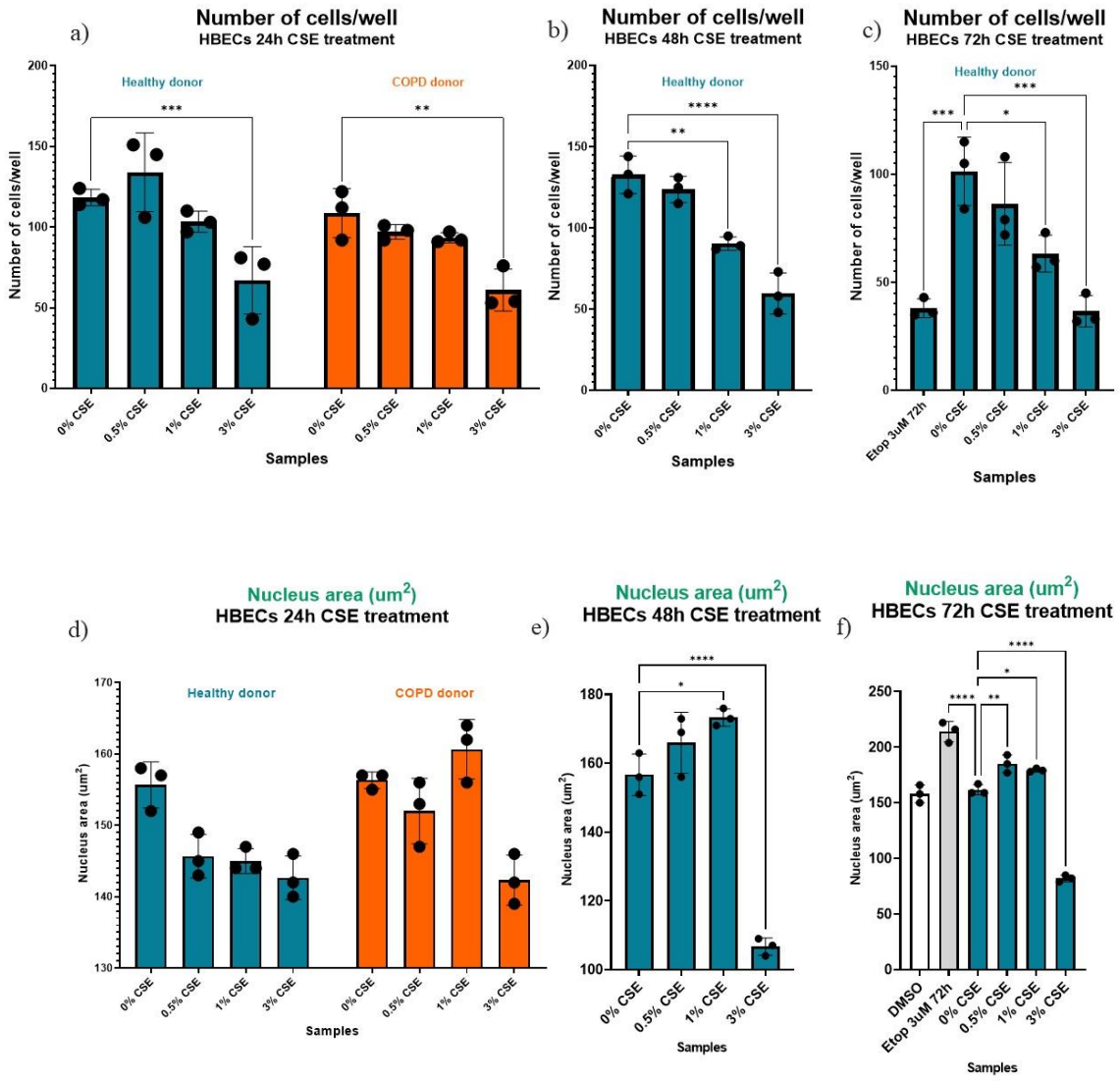

Fig 6. The cell death and nucleus area (μm²) for the HBECs from the healthy donor and COPD donor for the 24h to 72h time points. *A)-c) shows the nuclear death for the 24h, 48h and 72h respectively. D)-f) show the nucleus area (μm²) for the 24h, 48h and 72h. Both data sets are based upon the immunocytochemistry data which were run once, and with triplicates of each sample. Error bars in the graphs represent the SEM.*

Discussion

The aim of this project was to study autophagy and senescence in the context of COPD and different cell types. We wanted to investigate whether impaired autophagy and increased levels of senescence-associated markers correlated after CSE exposure in healthy and diseased lung cells.

Autophagy

To study autophagy flux in response to CSE exposure, we used autophagy markers p62 and LC3-II. Accumulation of both proteins suggests an impaired autophagy flux (Fujii et al., 2012; Kuwano, 2016; Pehote & Vij, 2020).

We found that both p62 and LC3-II accumulated after 5h and 24h of CSE exposure, and that this was the case in both donors (fig 2a-b, p. 13). Hence, the data suggests an impaired autophagy flux, which is consistent with previous literature (Fujii et al., 2012; Pehote & Vij, 2020). Fuji and colleagues showed a transiently impaired autophagy flux after 24h of 1% CSE exposure in HBECs. The same study found an elevated baseline activity in COPD donors, of both LC3-II and p62, compared to healthy donors (Fujii et al., 2012). Our data shows a similar pattern. In the immunoblotting data, the COPD donor had a higher p62 baseline level at the 5h time point (0% CSE; fig 2a, p. 13). However, for LC3-II, the baseline level was the same for the two donors, although the response started at a lower CSE concentration in the COPD donor, compared to the healthy (fig 2a, p. 13).

Another interesting find in our data, which also was reported by Fuji *et al*, was that the response in the COPD donor in the early time points is not as strong as for the healthy donor. In other words, the response can be described as attenuated in the COPD donor. Additionally, at the same time point (5h), an elevated baseline autophagy activity was observed (fig 2a, p. 13). This correlated with Fuji *et al* (Fujii et al., 2012). The already mentioned study speculates whether the response in the COPD donor is reduced due to impaired autophagy function and inability to respond to the same degree as healthy cells (Fujii et al., 2012). Another possibility could be a saturation of the autophagy system in these cells, due to an already strained system. In this case, it would be relevant to have gene expression data, in order to provide additional information into expression levels of these proteins. Hence, it would be a suitable additional experiment to perform in future studies.

In the later time points, 48h and 72h, increases in both p62 and LC3-II could be seen at 3% CSE concentration in both donors (fig 2c-d, p. 13). This data alone suggests an impaired autophagy flux at this concentration. However, when looking at the cells in the Yokogawa microscope, it is evident that the cells are distinctly different at the 3% CSE compared to the lower concentrations (fig 3c-f, p. 15-16). The cells are fewer, smaller in nuclear size and with an abnormal morphology. Possible causes could be that the combination of the CSE concentration and a long incubation time was toxic for the cells. Furthermore, the cells grew without media change for the full-time duration, and this could have given rise to starvation conditions and thereby cell death. To illuminate what was happening in the cells at this point, we can look at the senescence data.

Senescence

When investigating senescence, we used SA-β-Gal and cyclin inhibitor p21 as senescence-associated markers. They are both commonly used and are expected to increase with senescence - SA-β-Gal in the cytosol and p21 in the nucleus (Hamsanathan et al., 2019).

In our data, all investigated time points (24h, 48h and 72h) showed a significant increase in SA-β-Gal for the 3% CSE exposure. The lower concentrations of CSE gave rise to no or only slight SA-β-Gal expression (fig 4, p. 17-18). These results are in contrast to previous literature, in which Fuji *et al* showed an increase in SA-β-Gal even at 1% CSE (48h exposure time) (Fujii et al., 2012). However, in this case it is important to note that only one donor of each was used in our experiments. Additional donors and experiments would need to be run to determine if our contradictory pattern is donor-dependent or generally occurring. An additional study showed significant increase in SA-β-Gal positive cells at 10% CSE treated cells (duration time 6h) (Pehote & Vij, 2020). We did not investigate the 5h time point in our senescence experiments, since senescence is known to be a slow process and expected to appear at later time points, e.g. 48h. Pehote and Vij had a much higher CSE concentration than we did, which would explain the difference between our results. Additional experiments and more donors should be tested, to determine if our results are reproducible.

Regarding the p21 marker, the data is similar to SA-β-Gal at the 24h time point, showing a significant increase in p21 at the 3% CSE concentration (fig 5a, p. 19). In the later time points, the differences between the CSE concentrations are not evident. Instead, all CSE concentrations show an elevated p21 expression to more or less the same degree (fig 5b-c, p. 19). Fuji *et al* demonstrated an increase in p21 after 48h 1% CSE exposure using western blot (Fujii et al., 2012). We could not get the immunoblotting to work for p21 and therefore is no direct comparison possible. However, we did see an elevated p21 signal in our immunocytochemistry data and this corresponds to the previous literature (Fujii et al., 2012).

Important to note for the p21 data, is that the sample replicates showed large discrepancies. Furthermore, does the p21 localization change at the 3% CSE concentration, from being in the nucleus as expected, to being in the cytosol (fig 5d, p. 19). Whether this is due to that the function of p21 has changed or if this is an effect of e.g. high toxicity, needs to be further explored. One study suggested that the p21 localization to cytoplasm was correlated with anti-apoptotic pathways (Asada et al., 1999), however this research was done in a different cell type. More experiments with multiple donors are necessary to elucidate whether there is a general pattern of p21 localization to the cytoplasm in HBECs. However, in additional experiments it could be relevant to include apoptotic markers to investigate the prevalence and role of the process in this context. Senescence, apoptosis and autophagy has shown to be closely connected (Vicencio et al., 2008).

Additional to the senescence-associated markers, we estimated cell death and nucleus area based upon the immunocytochemistry data. Nucleus area is relevant to senescence since senescent cells have larger nucleus than normal cells (Hamsanathan et al., 2019; Muñoz-Espín & Serrano, 2014). Our data showed that the nucleus size increase significantly at both 48h and 72h (fig 6e-f, p. 20). However, at 3% CSE, the nucleus area drops drastically (fig 6e-f, p. 20). This indicates, just as with our other data, a different response at this concentration of CSE. Possibly, it could be due to too high toxicity of CSE and/or too long incubation time without media change. Interestingly though, it is this concentration that shows the highest levels of

senescence-associated markers. The senescence control etoposide showed a similar amount of cell death as 3% CSE, but instead an increase in nucleus area (fig 6c; fig 5f, p. 20). Thereby, we can conclude that senescent positive HBECs do exhibit enlarged nuclei and that the state of the 3% CSE exposed cells is unclear. Hence, further investigations are required to clarify the state of senescence in HBECs after exposure of CSE.

Concluding remarks

Conclusively, our data suggests transiently impaired autophagy at the early time points in HBECs, consistent with already published studies (Fujii et al., 2012; Pehote & Vij, 2020). Further experiments are needed to answer whether senescence occurs in these cells as well, as literature have suggested. Our aim was to correlate impaired autophagy and increased senescence-associated markers in the same cells. However, as the senescence data was partly unclear, it would be necessary to change the experimental design in the future. An altered experimental design which for example would include media change and fresh additions of CSE would decrease the risk of e.g. starvation effects or loss of potency of the CSE. Additional to this, could it be relevant to evaluate the bafilomycin control. The bafilomycin did not have a very strong effect on autophagy in the HBECs, and it would be relevant to work out the reasons for this – was it due to the bafilomycin substance itself or is it a recurrent event in HBECs?

With this project, we determined that CSE does impair autophagy in HBECs and that it can be successfully validated by immunoblotting and immunocytochemistry of p62 and LC3-II. Furthermore, we determined that SA-β-Gal is an appropriate senescence-associated marker in these cells. Since the project covered multiple time durations and different concentrations of CSE, it provided information regarding which time points and CSE concentrations that are of highest interest in the study of autophagy and senescence in HBECs using this model. With further optimization and with expansion in the use of donors, this *in vitro* model could be developed into an appropriate way to study the effects of CSE on primary human cells of different kinds. It can enable increased knowledge of autophagy and senescence in the context of COPD, but also contribute to the new research into medical targets, to improve and expand treatments of the disease.

Acknowledgements

I would like to thank the Target Science and Bioscience groups at AstraZeneca in Gothenburg for letting me be part of your teams. Especially, I would like to thank my supervisors Svitlana Salemio and Barry Collins for all their help and support during this thesis. I would also like to direct my thank you to the people at Lund University, for their support during the process of finishing the thesis: Christina Ledje, Wolfgang Knecht and David O'Carroll.

Lastly, I would like to thank my friends and family. I could not have finished this thesis without you.

References

Asada, M., Yamada, T., Ichijo, H., Delia, D., Miyazono, K., Fukumuro, K., & Mizutani, S. (1999). Apoptosis inhibitory activity of cytoplasmic p21Cip1/WAF1 in monocytic differentiation. *The EMBO Journal*, *18*(5), 1223–1234.

Blenis, J. (2017). TOR, the Gateway to Cellular Metabolism, Cell Growth, and Disease. *Cell*, *171*.

Cao, W. (2021). *An overview of autophagy: Mechanism, regulation and research progress*. 19.

Fujii, S., Hara, H., Araya, J., Takasaka, N., Kojima, J., Ito, S., Minagawa, S., Yumino, Y., Ishikawa, T., Numata, T., Kawaishi, M., Hirano, J., Odaka, M., Morikawa, T., Nishimura, S. L., Nakayama, K., & Kuwano, K. (2012). Insufficient autophagy promotes bronchial epithelial cell senescence in chronic obstructive pulmonary disease. *OncoImmunology*, *1*(5), 630–641.

Glick, D., Barth, S., & Macleod, K. F. (2010). Autophagy: Cellular and molecular mechanisms. *Journal of Pathology*, *221*, 3–12.

Hamsanathan, S., Alder, J. K., Sellares, J., Rojas, M., Gurkar, A. U., & Mora, A. L. (2019). Cellular Senescence: The Trojan Horse in Chronic Lung Diseases. *American Journal of Respiratory Cell and Molecular Biology*, *61*(1), 21–30. https://doi.org/10.1165/rcmb.2018-0410TR

Kawabata, T., & Yoshimori, T. (2020). Autophagosome biogenesis and human health. *Cell Discovery*, *6*(1), 33. https://doi.org/10.1038/s41421-020-0166-y

Kim, J., Kundu, M., Violett, B., & Guan, K.-L. (2011). AMPK and mTOR regulate autophagy through direct phosphorylation of Ulk1. *Nature Cell Biology*, *13*(2), 132–141.

Kocak, M. (2021). Targeting autophagy in disease: Established and new strategies. *Autophagy*.

Kuilman, T., Michaloglou, C., Mooi, W. J., & Peeper, D. S. (2010). The essence of senescence. *Genes and Development*, *24*, 2463–2479.

Kuwano, K. (2016). Cellular senescence and autophagy in the pathogenesis of chronic obstructive pulmonary disease (COPD) and idiopathic pulmonary fibrosis (IPF). *Respiratory Investigation*, *54*, 397–406.

Levine, B., & Kroemer, G. (2008). Autophagy in the Pathogenesis of Disease. *Cell*, *132*(1), 27–42. https://doi.org/10.1016/j.cell.2007.12.018

Matsunaga, K., Harada, M., Suizu, J., Oishi, K., Asami-Noyama, M., & Hirano, T. (2020). Comorbid Conditions in Chronic Obstructive Pulmonary Disease: Potential Therapeutic Targets for Unmet Needs. *Journal of Clinical Medicine, 9*(3078).

Muñoz-Espín, D., & Serrano, M. (2014). Cellular senescence: From physiology to pathology. *Nature Reviews Molecular Cell Biology*, *15*(7), 482–496. https://doi.org/10.1038/nrm3823

Nishimura, T. (2020). Emerging roles of ATG proteins and membrane lipids in autophagosome formation. *Cell Discovery*, *6*(32), 18.

Pankiv, S., Clausen, T. H., Lamark, T., Brech, A., Bruun, J.-A., Outzen, H., Øvervatn, A., Bjørkøy, G., & Johansen, T. (2007). P62/SQSTM1 Binds Directly to Atg8/LC3 to Facilitate Degradation of Ubiquitinated Protein Aggregates by Autophagy. *Journal of Biological Chemistry*, *282*(33), 24131–24145. https://doi.org/10.1074/jbc.M702824200

Pehote, G., & Vij, N. (2020). Autophagy Augmentation to Alleviate Immune Response Dysfunction, and Resolve Respiratory and COVID-19 Exacerbations. *Cells*, *9*(1952).

Racanelli, A. C. (2017). Autophagy and inflammation in chronic respiratory disease. *Autophagy*, *14*(2), 221–232.

Rodrigues, S. de O., Silva, P. L., Silva, A. R., & Gonçalves-de-Albuquerque, C. F. (2021). Mechanisms, Pathophysiology and Currently Proposed Treatments of Chronic Obstructive Pulmonary Disease. *Pharmaceuticals*, *14*(979).

Singh, D. (2017). Small Airway Disease in Patients with Chronic Obstructive Pulmonary Disease. *Tuberculosis & Respiratory Diseases*, *80*, 317–324.

Vicencio, J. M., Galluzzi, L., Tajeddine, N., Ortiz, C., Criollo, A., Tasdemir, E., Morselli, E., Younes, A. B., Maiuri, M. C., Lavandero, S., & Kroemer, G. (2008). Senescence, Apoptosis or Autophagy? *Gerontology*, *54*, 92–99.

Vij, N., Chandramani-Shivalingappa, P., Westphal, C. V., Hole, R., & Bodas, M. (2016). Cigarette smoke-induced autophagy impairment accelerates lung aging, COPD-emphysema exacerbations and pathogenesis. *The American Physiological Society*, *314*, C73–C87.

Wang, C., Jurk, D., Maddick, M., Nelson, G., & Martin-Ruiz, C. (2009). DNA damage response and cellular senescence in tissues of aging mice. *Aging Cell*, *8*, 311–323.

Wullschleger, S., Loewith, R., & Hall, M. N. (2006). TOR Signaling in Growth and Metabolism. *Cell*, *124*.

Yokogawa. (2023). *CellVoyager CV8000 High-Content Screening System*. Yokogawa.Com. https://www.yokogawa.com/eu/solutions/products-and-services/life-science/high-content-analysis/cv8000/#Overview

Zachari, M., & Ganley, I. G. (2017). The mammalian ULK1 complex and autophagy initiation. *Essays in Biochemistry*, *61*(6), 585–596. https://doi.org/10.1042/EBC20170021

Zhang, X. (2013). Why should autophagic flux be assessed? *Acta Pharmacologica Sinica*, *34*, 595–599.

Appendix

NHLFs: immunoblotting of p62 and LC3

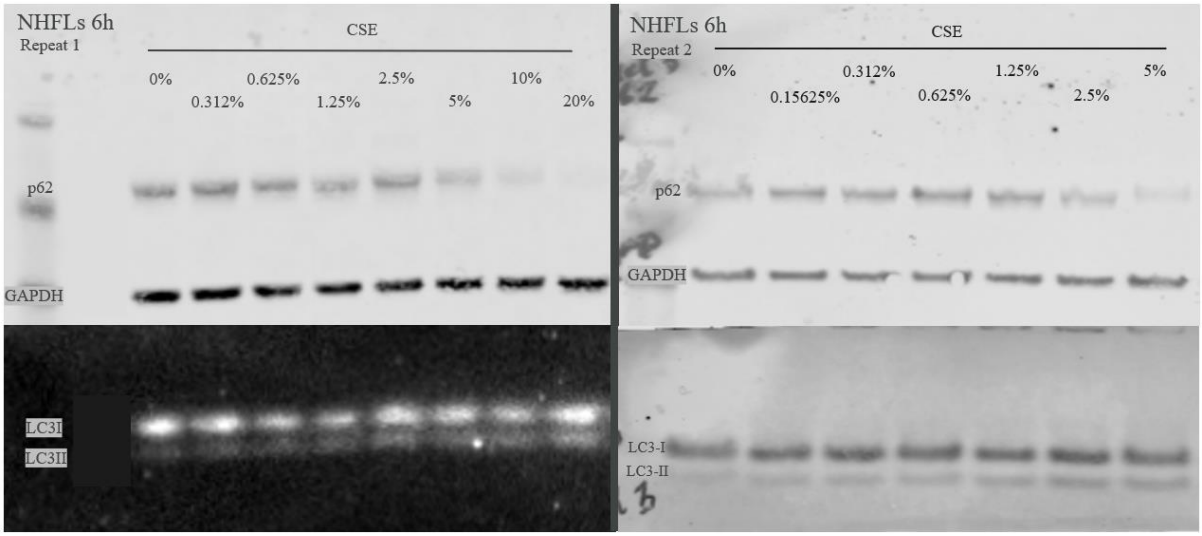

Fig 1. The immunoblotting data of the 6h time point of CSE exposure for the healthy NHLFs. The figure is showing the two repeated experiments, run with the same donor. To the left is the first repeat and to the right is the second. The two top gels show the p62 and GAPDH markers, while the bottom show LC3-I and LC3-II. The image to the bottom left is imaged by chemiluminescence and not Li-Cor.

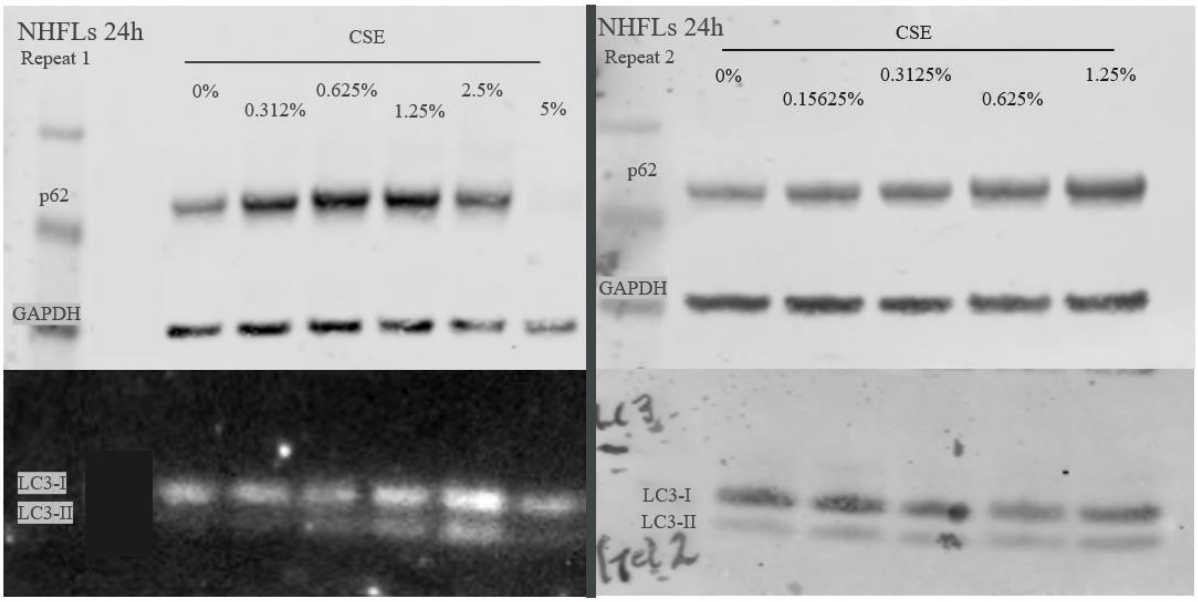

Fig 2. The immunoblotting data of the 24h time point of CSE exposure for the healthy NHLFs. As for the 6h time point (fig 1), this shows the two repeated experiments for the healthy NHLFs with p62 and GAPDH on the top and LC3-I and LC3-II on the bottom. The bottom left image is imaged by chemiluminescence, the rest with Li-COR.

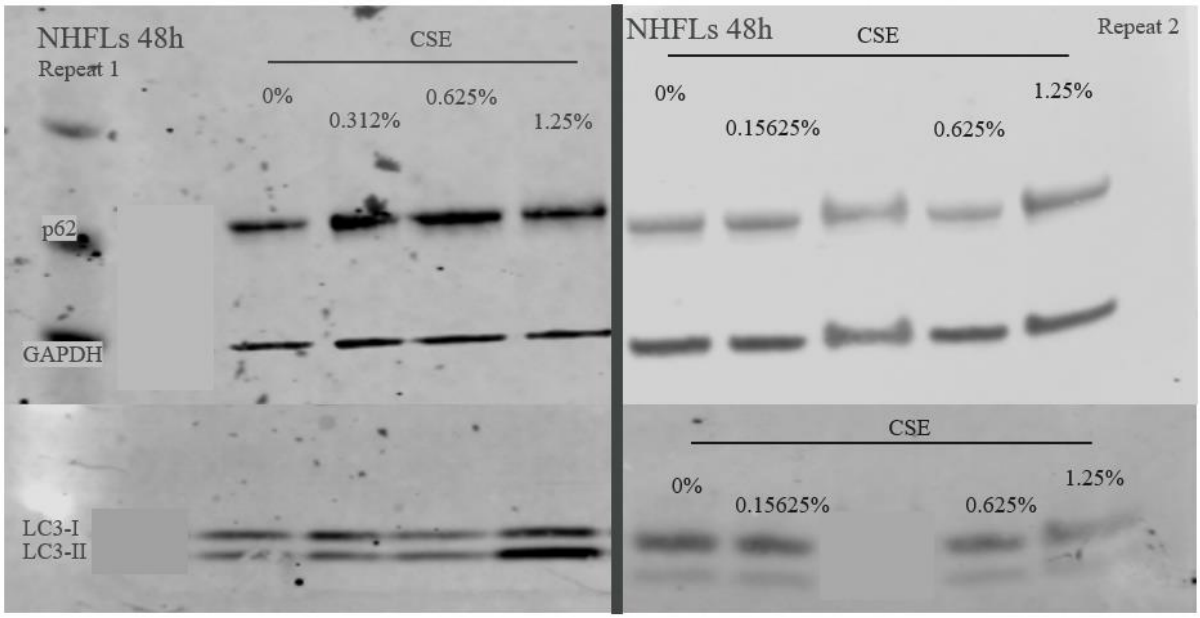

Fig 3. The immunoblotting data of the 48h time point of CSE exposure for the healthy NHLFs. Same lay out as for the two earlier figures, with two repeats of the same healthy donor. The p62 and GAPDH can be found on the top while the LC3-I and LC3-II in the bottom.

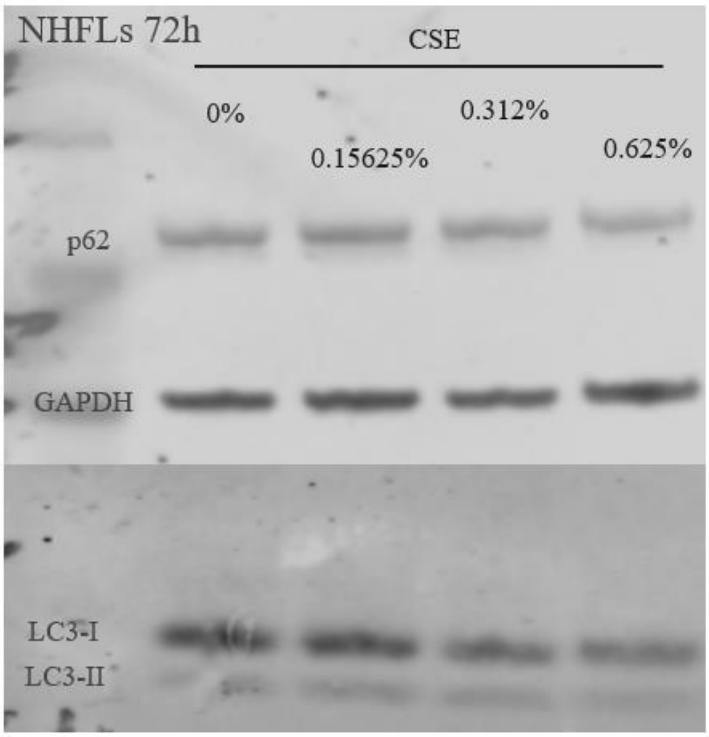

Fig 4. The immunoblotting data of the 72h time point of CSE exposure for the healthy NHLFs. This figure only shows one repeat of the time point, but otherwise the same set up as earlier figures. The p62 and GAPDH is found on the top while the LC3-I and LC3-II is found in the bottom.

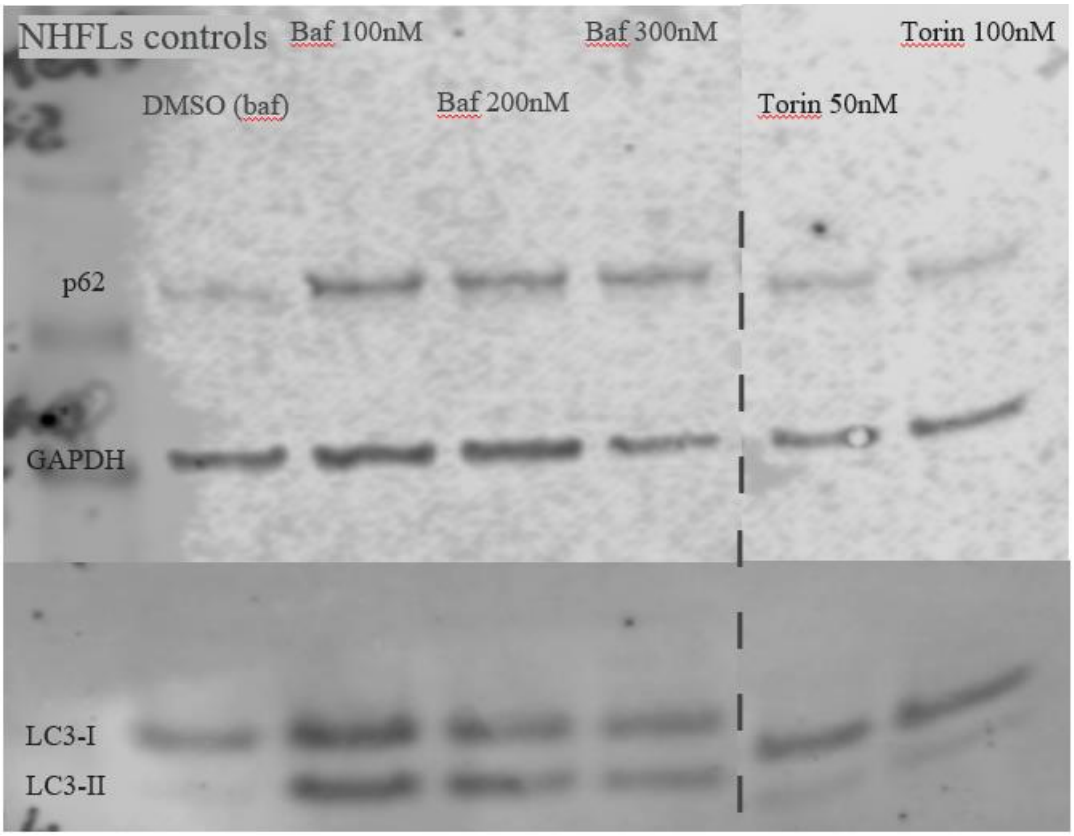

Fig 5. The immunoblotting data of the different controls used in the experiments with the healthy NHLFs. The figure shows one repeat of DMSO, different concentrations of bafilomycin (left) and two different concentrations of torin (right). At the top is the p62 and GAPDH while LC3-I and LC3-II can be found in the bottom.